Regular alumina-supported nanoparticles of iridium, rhodium and platinum under hydrogen reduction: structure, morphology and activity in the neopentane conversion

K. Hayek[a,*], H. Goller[b], S. Penner, G. Rupprechter[c], and C. Zimmermann[d]

[a]*Institut für Physikalische Chemie, Leopold-Franzens-Universität Innsbruck, Innrain 52A, A-6020 Innsbruck, Austria*
[b]*Sony Company, A-5020 Salzburg, Austria*
[c]*Fritz-Haber-Institut der Max-Planck-Gesellschaft, Faradayweg 4-6, D-14195 Berlin, Germany*
[d]*DSM Chemie Linz GmbH, St. Peter Str. 25, A-4021 Linz, Austria*

Received 11 August 2003; accepted 11 October 2003

Comparative studies of supported metal catalysts are facilitated if the catalysts consist of well-faceted metal particles whose structural changes under reaction conditions are known. We describe the use of regular noble metal crystallites (Ir, Rh and Pt), obtained by epitaxial growth on a single crystal (NaCl) substrate and subsequently contacted with the support by reactive high-vacuum deposition of the oxide, to study the inherent catalytic activity of the metals. Most of these metal particles exhibit defined zone axes parallel to the electron beam direction, which allows a characterization by selected area electron diffraction and lattice plane imaging in the electron microscope. The microstructural changes during activation processes (oxidation and reduction at temperatures up to 723 K) have been studied and correlated with corresponding changes in the conversion of neopentane with excess hydrogen. Particular emphasis was placed on the dependence of the reaction rates on hydrogen pressure. The structural changes at the metal–oxide interface upon reduction above ~673 K may be interpreted as a prestage to alloy formation.

KEY WORDS: heterogeneous catalysis; Ir; Rh; Pt; Al_2O_3; metal-support interaction; electron microscopy; structure-activity correlations; alloy formation.

1. Introduction

Comparative studies of the kinetics of hydrocarbon reactions on supported metals are generally impeded by the differences in structure, morphology and dispersion of the noble metal particles [1]. A meaningful evaluation of their catalytic properties would anticipate the occurrence of the different metals in identical or at least similar configurations (i.e. particle size and/or morphology) on the same oxide support. Owing to the fact that the rates of skeletal hydrocarbon reactions depend on a number of experimental variables, particularly on the hydrogen pressure [2] and on the reduction state of the support [3,4], a large set of experimental data must usually be accumulated before mechanistic conclusions can be drawn.

Some of these drawbacks can be overcome by investigating thin film model catalysts with well-shaped noble metal nanocrystals. The number of variables is reduced if the catalyst consists of defined regular metal particles whose structural changes under reaction conditions are known. (We define regular nanoparticles as polyhedra with an octahedral or cuboctahedral shape, in contrast to irregular particles with an undefined or hemispherical shape.) In our previous work [5–8], we described the use of well-faceted noble metal crystallites (Pt, Rh, Ir and Pd) obtained by epitaxial growth on a single crystal (NaCl) substrate and subsequently contacted with the support by reactive high-vacuum deposition of the oxide. Epitaxial growth on NaCl substrates results mainly in (001) contact faces of the metal; hence, after preparation for electron microscopy, the particles exhibit [001], or less frequently [011], zone axes parallel to the electron beam direction, which allows lattice plane imaging. Owing to their alignment, their characterization by selected area electron diffraction and by weak-beam dark-field imaging is facilitated. Model catalysts of different noble metals can be prepared with particles of similar size, shape and surface area, and their regular habit is a well-defined starting point to investigate and understand the microstructural changes during activation processes and during the catalytic reaction. On the other hand, supported metals grown epitaxially on large-area NaCl films provide sufficient surface area for kinetic measurements.

Thin-film model catalysts have been used in the past to discriminate between effects of particle size and of hydrogen pressure, which are frequently superposed [7,8], and also to monitor by electron microscopy the degree of metal-support interaction with increasing

* To whom correspondence should be addressed.
E-mail: konrad.hayek@uibk.ac.at

1011-372X/04/0100–0001/0

reduction temperature [8–11]. In particular, it could be shown that a treatment in 1-bar flowing hydrogen of regular Pt particles supported by ceria [9,10], silica [10,11] and alumina [10] induces alloy formation above a certain threshold temperature (about 723 K for ceria, 773 K for silica and 823 K for alumina). In each case, the simple cubic Pt_3Me alloy is formed as a first step, probably in a topotactic transition at the interface between the octahedral particle and the respective oxide. These results are a further proof that metal-support interaction is not limited to *reducible* oxides, but that it depends merely on the temperature of reduction, and that it determines the geometric arrangement at the metal-oxide interface [12–15].

In this work, we compare the structure, the structural changes and the catalytic activity of alumina supported on regular particles of iridium, rhodium and platinum, about 4–15 nm in size. Emphasis is placed on the effect of low-temperature reduction (LTR, below 773 K) where metal-support interaction is not extensive but still causes measurable activity changes. Transmission electron microscopy (TEM) at high resolution is again the main tool for monitoring the changes in structure and morphology, in particular, after regeneration and activation in oxygen and hydrogen. The catalytic activity is determined with reference to the neopentane reaction with emphasis on the dependence on hydrogen pressure.

The conversion of neopentane with hydrogen has attracted the attention of researchers for several reasons. The wealth of available kinetic data [16] allows the use of neopentane conversion as a test reaction for calibration purposes [17], or in attempts to define the state of a catalyst or of a support. While on most metals hydrogenolysis to methane and isobutane is the main initial step, platinum is able to isomerize the molecule with a high selectivity. Isomerization on Pt depends on the particle size, on the hydrogen pressure and on the support and its interaction with the metal [18–20]. It can occur via bond shift only and a number of mechanisms have been proposed in the past [18,21,22]. Isomerization with a lower selectivity also takes place on palladium, iridium and gold [20,23]. The selectivity of palladium and platinum can be altered by interaction with a support and by alloy formation [24], which has led several researchers to use the neopentane conversion as a tool to probe metal-support interaction [25,26].

2. Experimental

The preparation of the metal/Al_2O_3 films was performed in a high-vacuum chamber at a base pressure of 1×10^{-5} Pa. Nanosized particles were grown on NaCl (001) single-crystal faces by physical vapor deposition at substrate temperatures between 600 and 650 K. The mean particle size can be controlled by the nominal film thickness and by the deposition temperature. Two types of NaCl substrates were used for the preparation of the metal particles: vacuum-cleaved NaCl (001) single-crystal faces (0.25 cm^2) and *in situ* deposited NaCl films (up to 100 cm^2 surface area), the latter prepared by vapor deposition of NaCl on Cu sheets at 360 K. The structure of the respective metal particles is almost identical on the two substrates, except for some marginal particle coalescence occurring at the grain boundaries of the NaCl film substrate. The single crystal surfaces were cleaved *in vacuo* immediately before the metal deposition. The metal was evaporated by electron bombardment from the tip of a pure metal rod (Ir, Rh), or of a tungsten rod covered by the wire of the metal (Pt). The impinging flux was 1.2×10^{13} atoms cm^{-2} s^{-1} and the nominal film thickness was between 0.2 and 3 nm, monitored by a quartz crystal balance. Thereafter, the samples were cooled to room temperature in vacuum and covered with 25 nm of amorphous Al_2O_3 by reactive evaporation of Al in 10^{-2} Pa O_2 at a growth rate of 1 nm min^{-1} (Al metal was evaporated from a resistively heated Ta filament). For electron microscopy, one part of the resulting metal/oxide film was removed from the vacuum system, floated and rinsed in water and mounted on gold grids. For kinetic measurements, the film was further stabilized by depositing additional layers of alumina (or silica, up to 500 nm thick) on top, before it was removed from the NaCl substrate by floating in water, cleaned and mounted on quartz wool inside the reactor. The alumina film is amorphous and remains uncrystallized after treatment in oxygen or hydrogen up to 723 K, but it crystallizes after longer exposure to the electron beam in the microscope.

The structure and morphology of the metal particles and their changes due to oxidation and reduction at different temperatures were studied by high-resolution TEM and selected area electron diffraction in a Zeiss EM10 and a JEOL 4000EX microscope.

The reactions of neopentane and hydrogen were performed in a computer-controlled circulation reactor of about 16 mL volume described in [27]. It allows fast data acquisition and processing, so that an extensive and reproducible set of kinetic results can be obtained. The partial pressure of neopentane was varied between 5 and 20 mbar and the hydrogen pressure between 50 and 900 mbar, with helium gas always added up to 1 bar total pressure. The products were detected by gas chromatography with a flame ionization detector. From conversion versus time plots, the initial reaction rates were determined and the turnover frequencies (TOF) were calculated on the basis of free metal surface area (molecules per site per hour).

For a reference, some kinetic experiments were also performed on the standard EUROPT-1 catalyst (Pt/SiO_2, mean particle size 1.8 nm) for which a number of kinetic results are already available [28].

3. Results and discussion

3.1. Morphology and structure

On the sodium chloride substrate, all three noble metals grow in the Volmer–Weber mode as three-dimensional islands with a number density and size depending on the substrate temperature and on the deposition rate (for a detailed description of as-prepared samples and growth parameters see [5]). After deposition between 573 and 648 K, the particles are regularly shaped and very well oriented with respect to the substrate. Ninety percent of the Pt and Ir particles and 70% of the Rh particles exhibit (100) base planes parallel to NaCl (001), while most of the remaining particles are in (110) orientation. Model catalysts of this type generally exhibit a relatively narrow size distribution, with number densities ranging from 10^{10} to $10^{12}\,cm^{-2}$. The subsequent procedures, i.e., the coating with alumina and dissolution of the NaCl in water at room temperature, do not alter the morphology of Pt, Ir and Rh particles remarkably. The small particles in the "as-grown" state are, however, sensitive toward annealing and to gas exposure at elevated temperature, as described below. In general, several cycles of annealing in oxygen and hydrogen are required before a constant and reproducible catalytic activity is established. Upon these treatments, the particle size, shape and number density reach a steady state, which is maintained under the conditions of the subsequent catalytic reactions. The question that remains to be answered is to what extent the original (100) facets will survive as stable surface structures under the activation treatments, and also under the conditions of neopentane conversion for which (111) faces are more active [18,19]. Electron microscopy reveals that a low-temperature treatment in oxygen or hydrogen does not affect the (100) faces of larger (>5 nm) particles very much, but that it leads to exposure of other faces also to the ambient gas.

3.1.1. Iridium particles

Some examples for the structure and structural changes of iridium particles are given in figures 1–3.

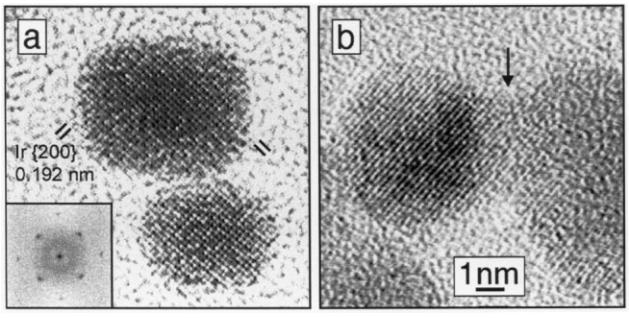

Figure 1. (a) Alumina-supported Ir nanoparticles in high resolution as grown and (b) after oxidation (1 bar O_2, 723 K, 30 min) and subsequent reduction in 1 bar hydrogen at 523 K . Insert: Fast Fourier transform of (a).

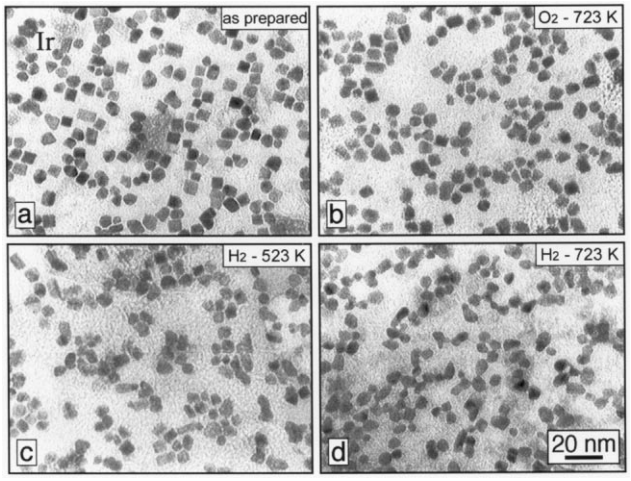

Figure 2. (a) Ir/Al_2O_3 model catalyst as grown and (b) after oxidation at 723 K for 120 min, (c) followed by reduction in 1 bar H_2 for 30 min at 523 K and (d) at 723 K.

Most as-grown particles are of squarelike appearance in the electron microscope at lower magnification. High-resolution images reveal mainly truncated half-octahedra (pyramids) with a (100) base plane (figure 1(a)). This shape remains unchanged upon exposure to oxygen (1 bar) at or below 823 K, but it is influenced by reduction in hydrogen. Upon exposure to hydrogen at 523 K, a "rounding" (correctly: faceting) of the particles is observed in the electron microscope, and neighboring particles tend to coalesce (figure 1(b)).

The series of electron micrographs in figure 2 show clusters of closely neighbored iridium particles in the as-grown state (a), after oxidation at 723 K (b), and after successive heating in hydrogen (c, d) (the images were taken from different sample spots). The particle outlines appear only slightly changed upon oxidation at 723 K (b) (in fact, a thin oxide skin around the particles could be observed in high resolution), whereas after reduction at 523 K (c), a number of particles appear rounded and coalesced with their close neighbors. Both coalescence and rounding have increased after reduction at 723 K (d). The changes of Ir particles are less pronounced than

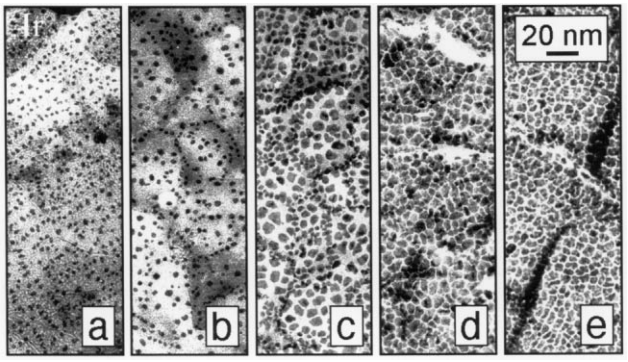

Figure 3. Iridium/alumina thin film catalysts Ir1–Ir5 after oxidation at 723 K and reduction at 573 K. Nominal Ir film thickness (a) 0.2 nm, (b) 0.4 nm, (c) 0.8 nm, (d) 2.0 nm and (e) 3.0 nm.

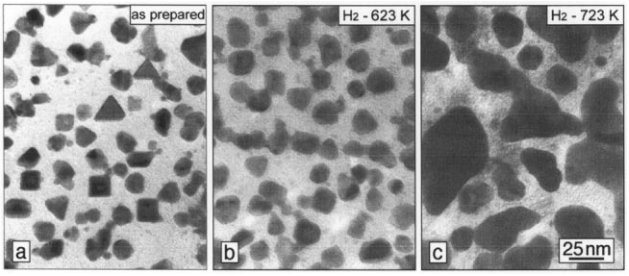

Figure 4. (a) Rh/alumina model catalyst, mean particle size 13.3 nm, as grown and (b) after oxidation at 673 K followed by reduction at 623 K and (c) 723 K.

the corresponding alterations of the less refractory metals Rh (figure 4) and Pt (figure 5). After several cycles of oxidation at 673 K and reduction at 523 K—which are most efficient for high and reproducible catalytic activity—the original epitaxial alignment is still partly preserved, as indicated by a (001)-texture in electron diffraction. However, the particles have changed to more irregular shapes, as shown also in figure 3. In this figure, five catalysts of different "nominal" Ir film thickness (0.2, 0.4, 0.8, 2.0 and 3.0 nm, also listed as Ir1 to Ir5 in table 1) are compared after a cycle of oxidation (673 K) followed by reduction (573 K). The mean particle size of the first three catalysts is 1.8, 2.1 and 4.3 nm, respectively. The two thicker samples are more densely packed and no mean particle size can be defined. The 3.0-nm Ir film (figure 3(e), "Ir5" in table 1) is almost continuous and has a columnlike structure. The accessible metal surface area depends on the pretreatment: in the as-grown state, it is identical to the sum of the base planes of the original polyhedra, but during activation, it increases because the particles are reshaped and the contact to the supporting alumina changes. Decoration of metal particles by the support that would lead to a decrease of active surface area does not occur on alumina upon reduction up to 723 K. A correlation of catalytic activity and particle surface must take into account the changes in surface area from the as-grown state (*initial* metal surface area, exposed base planes of the pristine particles, given for some catalysts in table 1) to the actual state, which was evaluated from the electron micrographs. The nominal dispersion D of the noncontinuous films can be estimated from the mean particle diameter. It represents the upper limit of accessible surface area and is also included in table 1.

3.1.2. Rh particles

The growth of Rh particles on NaCl surfaces has been described in [5], and their changes upon oxidation and reduction are documented in [6] and [8]. Epitaxial growth of Rh results in variously shaped particles, with predominant (100) orientation (>70%), followed by (110) orientation (20%). Upon exposure to oxygen up to 673 K, a thin surface oxide layer is formed around the particles without significant alteration of their shape. By a subsequent hydrogen treatment, this oxide layer is reduced and the particles are surrounded by facets that change from higher to lower Miller index with increasing temperature of reduction (up to 673 K). As an example, figure 4 shows a Rh/alumina catalyst of 13.3-nm mean particle size ("Rh2" in table 1) in its pristine state and after a standard activation in oxygen followed by reduction in hydrogen at 623 K and 723 K respectively. After reduction at 623 K, the original (100)

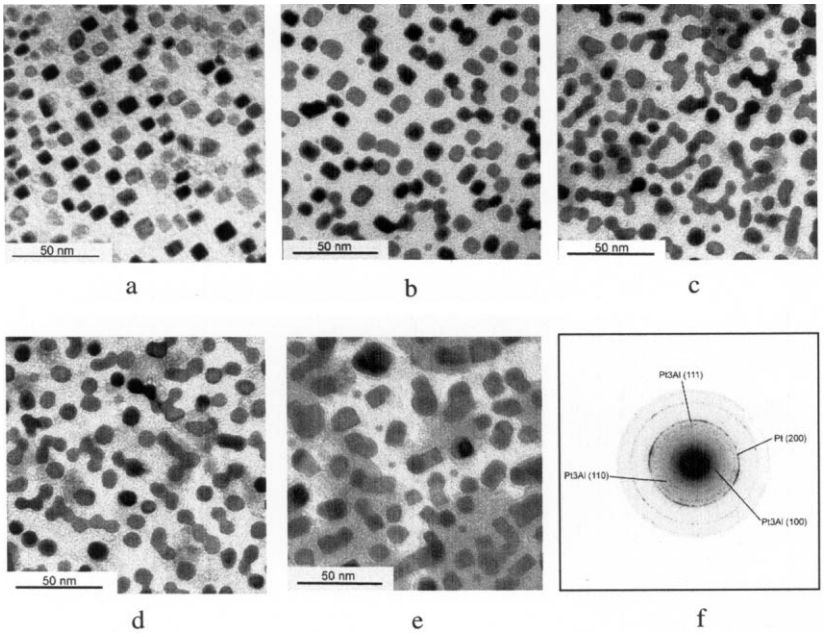

Figure 5. Pt/alumina model catalyst, mean particle size 7.8 nm, as grown, and after oxidation at 673 K, followed by reduction in 1-bar hydrogen for 30 min at 673 K, 773 K, 823 K and 873 K. The selected area electron diffraction pattern indicates alloy formation (Pt_3Al) after reduction at 873 K.

Table 1
Characteristics of Ir- and Rh-Al_2O_3 model catalysts. Pretreatment: 1 bar O_2, 723 K; 1 bar He, 298 K; 1 bar H_2, 523 K. Reaction: $P_{NP} = 5$ mbar, P_{H_2} as indicated, He added to 1 bar total pressure, $T = 473$ K

Catalyst, mean particle size (nominal metal thickness)	("Initial") total number of exposed surface atoms	Dispersion (nominal)	P_{H_2} of maximum TOF (mbar)	Maximum TOF (h^{-1})[a]
Ir1, 1.8 nm (0.2 nm)	1.7×10^{16}	0.61	300	27
Ir2, 2.1 nm (0.4 nm)	2.0×10^{16}	0.52	300	18
Ir3, 3.4 nm (0.8 nm)	6.0×10^{16}	0.32	150	18
Ir4, almost continuous film (2.0 nm)	1.0×10^{17}	~0.09	100	80
Ir5, continuous film (3.0 nm)	1.2×10^{17}	~0.06	50	85
Rh1, 7.8 nm (0.8 nm)	1.2×10^{16}	0.14	100	90
Rh2, 13.3 nm (2.4 nm)	2.2×10^{16}	0.08	100	107
Rh3, 16.7 nm (4.2 nm)	$3.4^{a} \times 10^{16}$	0.06	100	100

[a]TOF given in molecules per metal site per hour.

alignment is still retained, but the particles are more irregularly shaped than in the as-grown state. After an increase of the reduction temperature to 723 K (figure 4(c)), the Rh metal has started to wet the alumina substrate and particle coalescence has occurred. The onset temperature of spreading and coalescence depends on the Rh metal loading, but is always about 100 K higher than on a comparable Rh/titania model catalyst [8]. At even higher reduction temperature, Rh/Al alloy formation, like on Pt/alumina, might be expected [10], but in the present experiments, the temperature of hydrogen prereduction (T_{red}) was always kept below 723 K. Three Rh model catalysts of different metal loading are included in table 1 for a comparison with iridium.

3.1.3. Pt particles

As discussed earlier [5,29,30], most as-grown Pt particles are truncated half-octahedra in a (100) orientation to the substrate (i.e. they expose predominantly (100) faces to the reactants). Activation in oxygen followed by reduction in hydrogen (LTR) leads to faceting of corners and finally to an increased proportion of (110) faces participating in the reaction, as described e.g., in [31]. The series of images in figure 5 shows the transition with increasing reduction temperature from the as-grown state of Pt-Al_2O_3 to the formation of the Pt_3Al alloy, which is reached at about 873 K [10]. EXAFS studies by Koningsberger *et al.* of small Pt particles on Al_2O_3 [12–15] have revealed a difference in the Pt–O distance after low- and high-temperature hydrogen reduction. Likewise, these authors observed that the ratio of adsorbed H atoms per surface Pt atom was above unity after LTR and confirmed this by temperature-programmed desorption (TPD). The extra hydrogen between the metal particle and the support ("hydrogen cushion" [13,14]) is removed by subsequent reduction at 723 K, and stronger Pt–O bonds are formed. In figure 5, it is seen that the rounding of particles and the degree of wetting between Pt and alumina increase after low-temperature reduction and then decrease again under high-temperature reduction. At the final stage (figure 5(e), after reduction at 873 K), the sharp edges of some particles are characteristic of a Pt_3Al alloy, which coexists with other Pt-rich alloy phases and possibly also with unreacted Pt [10].

3.2. Kinetic measurements

As mentioned before, of the three metals, Pt isomerizes neopentane to a significant extent, while hydrogenolysis occurs on Ir preferentially and on Rh exclusively. A meaningful comparison of the hydrogenolysis activities at the same reaction temperature is possible for Rh and Ir, but not for Pt with its orders of magnitude lower overall activity.

3.2.1. Neopentane reaction on iridium and rhodium

Isomerization

On the Ir catalysts, isomerization products of neopentane (isopentane and traces of *n*-pentane) appeared primarily at the early reaction stages, but were rapidly consumed thereafter. The extent of isomerization was favored by higher partial pressures of hydrogen and by increasing particle size, but never exceeded 5% of the overall conversion. This is in agreement with results reported previously [20,23,33] and is not further discussed here. As expected [20], on the rhodium catalysts, isomerization was not detected.

Hydrogenolysis—dependence on P_{NP} and P_{H_2}

Table 1 contains characteristic data of the five Ir catalysts (Ir1–Ir5) imaged in figure 3 and of three Rh model catalysts of different mean particle size (Rh1–Rh3), together with their highest catalytic activities measured at 473 K, obtained after a preoxidation at 723 K followed by a low-temperature reduction at 523 K. The order in neopentane, measured at 473 K and constant hydrogen pressures of 50 to 300 mbar, was

positive (approximately unity) at low neopentane pressures ($P_{NP} > 10$ mbar), then changed to zero in the region of 10 mbar, and was negative at higher P_{NP}.

The dependence of the reaction rates on P_{H_2} was thus always determined at low P_{NP}. At a given hydrocarbon pressure, the activity passed a maximum as a function of P_{H_2}. The TOF of the three highly dispersed Ir catalysts (Ir1–Ir3) are lower and comparable, but the rates on the low-dispersed catalysts Ir4 and Ir5 are up to five times higher and similar to those of the three Rh catalysts of equal (low) dispersion. An increase of the reduction temperature from 523 to 723 K resulted in an activity decrease by about 80% on *all* catalysts, which is also in agreement with reports in the literature [23,33].

In figure 6, the course of neopentane reactions at a given hydrocarbon pressure is shown for the two catalysts Ir3 (3.4 nm mean particle size, (a)) and Rh1 (particle size 7.8 nm, (b)) (reaction temperature 473 K, hydrocarbon pressure 5 mbar, hydrogen pressure varied between 50 and 900 mbar). The reaction rates and the product distributions, and also the dependence of either on the hydrogen pressure are well comparable. At constant hydrocarbon pressure, the reaction rates on the Ir and Rh catalysts pass a relatively narrow maximum as a function of P_{H_2}. Under the given conditions, these

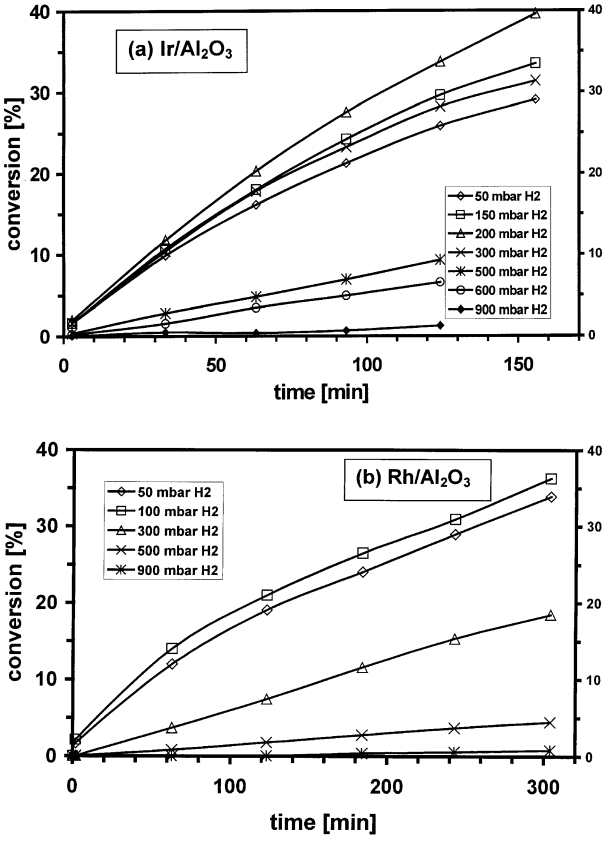

Figure 6. (a) Reaction of 5-mbar neopentane with variable pressures of hydrogen on Ir/alumina (3.4 nm particle size) and (b) Rh/alumina (7.8 nm mean particle size) at 473 K. Helium added to 1 bar total pressure.

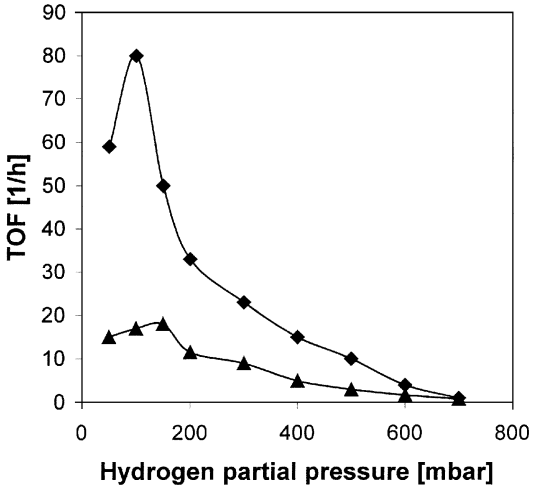

Figure 7. Initial turnover rate of neopentane conversion versus hydrogen partial pressure. Reaction conditions: 5-mbar neopentane, helium added to 1 bar total pressure, 473 K; ▲ catalyst Ir3, ◆ catalyst Ir4.

maxima are located near 200-mbar hydrogen pressure for Ir3 and near 100-mbar hydrogen for Rh1. The initial TOF of the catalysts Ir3 and Ir4 versus the hydrogen partial pressure at a neopentane pressure of 5 mbar and a reaction temperature of 473 K are plotted in figure 7. The hydrogen pressure at which the maxima of TOF are observed are summarized in table 1. It is seen that with increasing Ir particle size, the TOF maximum is shifted toward lower P_{H_2}, e.g., at 473 K from about 300 mbar (Ir1) to 50 mbar (Ir5). With increasing reaction temperature, all maxima move toward higher P_{H_2}. On the Rh samples, the conversion was nearly independent of particle size on the studied catalysts (observed TOF maximum always near 100 mbar H_2), but this apparent absence of a particle size effect may also be due to the relatively low and similar dispersion of the three catalysts.

Previously, mainly negative orders in hydrogen (up to −3) have been observed for hydrogenolysis on Ir [32] and on some other noble metals [20,34]. However, in most cases, the studied range of hydrogen pressure was presumably too narrow to discover a maximum in the hydrogen pressure versus activity plot, which would be expected e.g., from a simple Langmuir–Hinshelwood approach. The present experiments yield a positive order in H_2 at low pressures and an activity maximum at a hydrogen excess of about 10 : 1 at 473 K. Beyond the maximum, the hydrogen order decreases with increasing hydrogen pressure, and between 300 and 700 mbar H_2, a value between −2.5 and −3 is approached. This is an indication of a more dehydrogenated intermediate as proposed by Menacherry and Haller [26], but may also be due to an ensemble size effect as postulated by Frennet *et al.* [35].

As a consequence of the observed hydrogen pressure dependence, the apparent activation energy of hydrogenolysis on Ir must also be P_{H_2} dependent and must

Table 2
Reactivity and selectivity of a Pt-Al_2O_3 model catalyst, mean particle size 4 nm, in the conversion of neopentane and products. Reaction temperature 623 K, hydrocarbon pressure 20 mbar, hydrogen pressure as indicated, with He added to 1 bar total pressure. Catalyst pretreatment: 1 bar oxygen at 673 K, followed by 1 bar hydrogen at 573 K

	P_{H_2} (mbar)	Initial TOF (h^{-1})	Selectivity (initial ratio isomerization/hydrogenolysis)
Neopentane	400	151	1.2
Neopentane	600	127	1.2
Neopentane	800	16	2.0
Isopentane	200	58	1.6
Isopentane	400	302	2.7
Isopentane	800	331	1.6
Isobutene	600	222	5.6
Isobutene	800	102	4.9
Propane	400	91	
Propane	600	27	
Propane	800	15	
Ethane	800	0.44	
Neopentane (on EUROPT−1)	400	57	0.42

increase with P_{H_2} in the high-pressure range. Indeed, the energies of activation measured between 373 and 523 K vary between 100 and 200 kJ in the hydrogen pressure range between 50 and 700 mbar. At partial pressures of 200-mbar H_2 and 5-mbar neopentane, an E_a of $135 \pm 4\,kJ\,mol^{-1}$ was determined on the three Ir catalysts.

The product distribution on Rh and Ir is very similar. Initially, only methane and isobutane are formed (besides small amounts of isopentane on Ir), but with increasing conversion, the proportion of isobutane in the products decreases and propane and ethane are formed in secondary reactions, whereby the decay of isobutane is again a function of hydrogen pressure. This confirms the previously proposed mechanism of consecutive demethylation [25,36,37].

As mentioned before, the hydrogenolysis activity decreases with reduction temperature up to 723 K. This may be explained by a change of the surface structure of the metal particles as discussed previously for the case of alumina-supported Rh particles [8]. Their activity decrease with reduction temperature could be correlated with the decrease of surface roughness due to the formation of lower-index facets. On the other hand, the reduction of Ir/alumina at 723 K has led to increased wetting at the Ir/alumina interface, as presented in figure 2(d). In accordance with the corresponding observations on Pt/Al_2O_3 [13,14], this is an indication of increased metal-support interaction.

3.2.2. Neopentane reactions on platinum

Owing to the lower reactivity and the small surface area of the thin-film model catalysts, the reactions on Pt were performed at higher temperatures (573 K and above), and the range of prereduction temperature for studying metal-support interaction is therefore limited to 573 to 723 K. In this temperature regime and under excess of hydrogen, the observed reaction order in neopentane was slightly positive (≤ 0.3), (compared to 0.8–0.9 reported by Leclercq *et al.* [34] for impregnated Pt/alumina). In a previous kinetic study on thin-film model catalysts [29,30], we have reported changes of the isomerization selectivity as a function of size and orientation of the regular Pt particles. For a better understanding of the complex product distribution, detectable already at the beginning of the reaction, we investigated the hydrogen pressure dependence of the conversion of neopentane and its products on a model Pt catalyst of 4-nm mean particle size at 623 K (table 2). At a given hydrocarbon pressure (in the present case 20 mbar), the rate of neopentane conversion passes a broad maximum near 400 mbar H_2, followed by an initially slow and then more rapid decrease. The selectivity toward isomerization is about 55% at 400 mbar and increases with P_{H_2}. On the other hand, the hydrogen pressure dependence of the conversion of the primary products of hydrogenolysis (isobutane) and of isomerization (isopentane) is markedly different, as seen in table 2. The varying conversion rates of the products with hydrogen pressure will result in a changing product spectrum not only during the course of each reaction but also in the initially detectable stage. Furthermore, as stated by Sarkany *et al.* [33], the slow desorption of products is also a reason for the multiple rupture of C–C bonds. In addition, it must be noted that the individual reaction rates of the primary and secondary products again depend on the particle size and structure of the catalyst.

4. Conclusions

The main intention of this paper is to prove that thin-film model catalysts are a useful tool for comparing the

inherent catalytic activities of different metals under a variety of experimental conditions. Since the metal particles exhibited the same polyhedral shape (independent of the metal), structural differences typically originating from different growth modes could be excluded. It could be shown that thin-film model catalysts offer the possibility of monitoring structural changes by TEM and also facilitate the comparison of hydrogen and hydrocarbon pressure dependence of the reactions of neopentane (and of its primary products). The studied model systems were Ir, Rh and Pt particles of comparable size embedded in an amorphous alumina support. The TOFs of neopentane hydrogenolysis depend on the catalyst dispersion and also very strongly on the hydrogen pressure. A comparison with previous results from is difficult because of the various types of catalysts reported in the literature (powdered metals, different supports, etc. [38]). However, our data show that the conversion rates of neopentane and some other hydrocarbons on the three metals (Ir, Rh and Pt) always pass a maximum as a function of hydrogen pressure, which may depend on the particle size and is shifted to higher hydrogen pressure with increasing temperature.

Finally, it is of interest to compare the kinetic results obtained on model catalysts with those of neopentane conversion measured under ultrahigh vacuum (UHV) or UHV-compatible conditions. For instance, on a clean Rh foil, Reichl [39] measured an initial turnover rate of $42\,h^{-1}$ at 471 K and at partial pressures of 8-mbar neopentane and 80-mbar hydrogen, which is in good agreement with the range reported here. Engstrom *et al.* [40] showed that the specific rates of hydrogenolysis on Ir (111) and $(110)-1\times2$ single-crystal surfaces are orientation dependent. Nevertheless, the reported turnover rates at 475 K and comparable neopentane/hydrogen pressures again range between 36 and $100\,h^{-1}$. Furthermore, the early experiments by Somorjai *et al.* [19] on single-crystal faces of Pt ((100), (111) and stepped/kinked surfaces) indicate a strong dependence of hydrogenolysis and isomerization rates on the orientation and the roughness of the crystal face.

A last point to be discussed is the structural alterations of the different metal particles under "low-temperature" reduction up to 723 K. It has to be kept in mind that they can be observed only at high metal loading, i.e., on relatively large and closely spaced metal particles. Changes of the interfacial tension between metals and *reducible* oxides are usually correlated with the formation of lower-valent cations and oxygen vacancies at the metal-oxide interface. The observed coalescence and spreading phenomena occurring under hydrogen reduction of Ir (523–723 K, figure 2), Rh ($\geq$623 K, figure 4) and Pt ($\geq$673 K, figure 5) on "nonreducible" alumina require an assessment of the reduction state of the support. Earlier, Kunimori *et al.* [41] have proposed the formation of Pt-Al_2O_2 species at the interfaces, whereas Vaarkamp *et al.* [13,14] discovered a changing Pt–O distance with increasing reduction temperature. According to our recent findings, the Pt–Al alloy formation on thin-film model systems starts at much lower temperature than previously expected ($\leq$873 K) [10]. Cubic Pt_3Al seems to be formed in the first step, probably because of the facilitated topotactic pathway and the intense metal-oxide contact. Owing to their regular habit, Pt_3Al particles might represent an interesting model system for studies of structure–activity correlations in selected reactions, but so far, it has not been possible to exclude the parallel formation of less regular particles of other alloys. It is very likely that prestages of alloy formation will also occur on the other two metals (Ir, Rh) in a corresponding temperature range, which may be a topic of future research.

Acknowledgments

This work was supported by the Austrian Science Fund (Project S 8105) and by the National Bank of Austria (Project 6676/2).

References

[1] J.R. Anderson, Adv. Catal. 23 (1973) 1.
[2] Z. Paál and P.G. Menon (eds), *Hydrogen Effects in Catalysis* (Marcel Dekker Inc., Vienna and Basel, 1988).
[3] S.J. Tauster and S.C. Fung, J. Catal. 55 (1978) 29.
[4] G.L. Haller and D.E. Resasco, Adv. Catal. 36 (1989) 173.
[5] G. Rupprechter, K. Hayek, L. Rendón and M. José-Yacamán, Thin Solid Films 260 (1995) 148.
[6] G. Rupprechter, K. Hayek and H. Hofmeister, J. Catal. 173 (1998) 409.
[7] C. Zimmermann and K. Hayek, in *New Frontiers in Catalysis*, Proc. 10th Int. Congress on Catalysis, Budapest, 1992, L. Guczi *et al.* (eds) (Elsevier, Amsterdam 1993) p. 2375.
[8] G. Rupprechter, G. Seeber, H. Goller and K. Hayek, J. Catal. 186 (1999) 201.
[9] S. Penner, G. Rupprechter, H. Sauer, D.S. Su, R. Tessadri, R. Podloucky, R. Schlögl and K. Hayek, Vacuum 71 (2003) 71.
[10] S. Penner, D. Wang, D.S. Su, G. Rupprechter, R. Podloucky, R. Schlögl and K. Hayek, Surf. Sci. 532-535 (2003) 276.
[11] D. Wang, S. Penner, D.S. Su, G. Rupprechter, K. Hayek and R. Schlögl, J. Catal. in press.
[12] A. Munoz-Páez and D.C. Koningsberger, J. Phys. Chem. 99 (1995) 4193.
[13] M. Vaarkamp, F.S. Modica, J.T. Miller and D.C. Koningsberger, J. Catal. 144 (1993) 611.
[14] M. Vaarkamp, J.T. Miller, F.S. Modica and D.C. Koningsberger, J. Catal. 163 (1996) 294.
[15] B.L. Mojet, M.J. Kappers, J.T. Miller, D.C. Koningsberger, *Proc. 11th Int. Congr. Catal.* Baltimore, 1996, Part B (Elsevier, Amsterdam, 1996) p. 1165.
[16] G.A. Somorjai, *Introduction to Surface Chemistry and Catalysis* (John Wiley and Sons Inc., New York 1994).
[17] G.C. Bond, F. Garin and G. Maire, J. Catal. 41 (1988) 313.
[18] J.R. Anderson and N.R. Avery, J. Catal. 5 (1966) 466; 7 (1967) 315.
[19] S.M. Davis, F. Zaera and G.A. Somorjai, J. Am. Chem. Soc. 104 (1982) 7453.
[20] M. Boudart and L.D. Ptak, J. Catal. 16 (1970) 90.

[21] J.K.A. Clarke and J.J. Rooney, Adv. Catal. 25 (1976) 125.
[22] F.G. Gault, Adv. Catal. 39 (1981) 125.
[23] Z. Karpinski, W. Juszczyk and J. Pielaszek, J. Chem. Soc., Faraday Trans. I 83 (1987) 1293.
[24] W. Jusczyk and Z. Karpinski, J. Catal. 117 (1989) 519.
[25] Z. Karpinski, Z. Zhang and W.M.H. Sachtler, Catal. Lett. 13 (1992) 123.
[26] P.V. Menacherry and G.L. Haller, J. Catal. 167 (1997) 425.
[27] C. Zimmermann and K. Hayek, Chem. Ing. Tech. 63 (1991) 68.
[28] G.C. Bond, F. Garin and G. Maire, Appl. Catal. 41 (1988) 313.
[29] E. Gehrer and K. Hayek, J. Mol. Catal. 39 (1987) 293.
[30] K. Hayek, J. Mol. Catal. 51 (1989) 347.
[31] G. Rupprechter, J.J. Calvino, C. López-Cartes, M. Fuchs, J.M. Gatica, J.A. Pérez-Omil, K. Hayek and S. Bernal, Stud. Surf. Sci. Catal. 130 (2000) 2021.
[32] K. Foger and J.R. Anderson, J. Catal. 59 (1979) 325.
[33] A. Sárkány, K. Matusek and P. Tétényi, J. Chem. Soc. Faraday Trans. 73 (1977) 1699.
[34] G. Leclercq, L. Leclercq and R. Maurel, J. Catal. 44 (1976) 68.
[35] A. Frennet, G. Liénard, A. Crucq and L. Degols, J. Catal. 53 (1978) 150.
[36] H.C. Yao and M. Shelef, J. Catal. 56 (1979) 12.
[37] Z. Karpinski, W. Butt and W.M.H. Sachtler, J. Catal. 119 (1989) 521.
[38] G.A. Somorjai, *Introduction to Surface Chemistry and Catalysis* (Wiley, New York 1994), p.540, 541 and 573.
[39] W. Reichl, Diploma Thesis, University of Innsbruck, 1996.
[40] J.R. Engström, D.W. Goodman and W.H. Weinberg, J. Am. Chem. Soc. 110 (1988) 8305.
[41] K. Kunimori, Y. Ikeda, M. Soma and T. Uchijima, J. Catal. 79 (1983) 185.